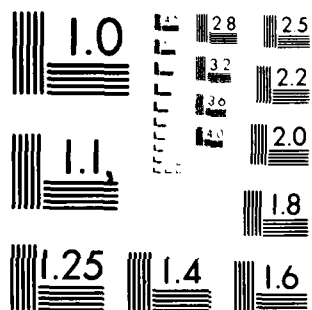END
DATE
FILMED

9 83

DTIC

MICROCOPY RESOLUTION TEST CHART

NATIONAL BUREAU OF STANDARDS-1963-A

ADA131868

A MODEL FOR CHORUS ASSOCIATED ELECTROSTATIC BURSTS

by

Crockett L. Grabbe

DTIC
SELECTED
AUG 2 6 1983
A

Department of Physics and Astronomy

THE UNIVERSITY OF IOWA

Iowa City, Iowa 52242

83 08 24 003

A MODEL FOR CHORUS ASSOCIATED ELECTROSTATIC BURSTS

by

Crockett L. Grabbe

June 1983

Department of Physics and Astronomy
The University of Iowa
Iowa City, IA 52242

REPORT DOCUMENTATION PAGE		READ INSTRUCTIONS BEFORE COMPLETING FORM
1. REPORT NUMBER U. of Iowa 83-23	2. GOVT ACCESSION NO. AD-A131868	3. RECIPIENT'S CATALOG NUMBER
4. TITLE (and Subtitle) A MODEL FOR CHORUS ASSOCIATED ELECTROSTATIC BURSTS		5. TYPE OF REPORT & PERIOD COVERED Progress June 1983
		6. PERFORMING ORG. REPORT NUMBER
7. AUTHOR(s) CROCKETT L. GRABBE		8. CONTRACT OR GRANT NUMBER(s) N00014-76-C-0016
9. PERFORMING ORGANIZATION NAME AND ADDRESS Department of Physics and Astronomy The University of Iowa Iowa City, IA 52242		10. PROGRAM ELEMENT, PROJECT, TASK AREA & WORK UNIT NUMBERS
11. CONTROLLING OFFICE NAME AND ADDRESS Electronics Program Office Office of Naval Research Arlington, VA 22217		12. REPORT DATE 30 June 1983
		13. NUMBER OF PAGES 29
14. MONITORING AGENCY NAME & ADDRESS(If different from Controlling Office)		15. SECURITY CLASS. (of this report) UNCLASSIFIED
		15a. DECLASSIFICATION/DOWNGRADING SCHEDULE

16. DISTRIBUTION STATEMENT (of this Report)

Approved for public release; distribution is unlimited.

17. DISTRIBUTION STATEMENT (of the abstract entered in Block 20, If different from Report)

18. SUPPLEMENTARY NOTES

Submitted to J. Geophys. Res.

19. KEY WORDS (Continue on reverse side if necessary and identify by block number)

Electrostatic Bursts
Plasma Instability
Resistive Medium Instability
Electrons
Chorus Wave Packet

20. ABSTRACT (Continue on reverse side if necessary and identify by block number)

(See following page)

ABSTRACT

The linear theory of the generation of electrostatic bursts of noise by electrons trapped in chorus wave packets is developed for a finite temperature electron beam and a Maxwellian electron and ion background. The growth rates determined are qualitatively in good agreement with those obtained by previous authors from a more idealized model. Two connected instability mechanisms seem to be occurring: a beam plasma (electron-ion two-stream) instability commonly associated with intensification of the chorus power levels, and a transitional or borderline resistive medium instability commonly associated with chorus hooks. The physical reasons for the two mechanisms is discussed. In the second case electron beams are difficult to identify in the particle data. An expression is obtained for the maximum growth rate in terms of the ratios of the beam and electron thermal velocities to the beam velocity, and of the beam density to plasma density. It is anticipated that this may allow the observed peak in the electrostatic noise spectrum to be used as a diagnostic for the beam characteristics.

I. INTRODUCTION

In recent papers, Reinleitner et al. [1982; 1983] presented data showing the generation of electrostatic waves by electrons trapped in chorus wave packets. This was explained on the basis that the phase velocity of the chorus wave packet changes with the local plasma conditions and magnetic field, resulting in acceleration of the trapped particles. The acceleration process was considered in more detail in a more recent paper [Gurnett and Reinleitner, 1983]. Acceleration shifts the trapped particles in velocity space, so that they produce a "bump" (beam) superimposed on the untrapped or background electrons. Thus, a beam instability results that can drive electrostatic waves.

The model that Reinleitner et al. used to compute the spectrum produced by the instability was that of a resonance (Lorentzian) distribution of electrons and a delta function (zero temperature) beam distribution in velocity space. From this they concluded that a "resistive medium" (negative energy) beam instability was involved. It is the purpose of the present paper to develop the theory from a more realistic model with the objective of putting the interpretation of the data on a firmer foundation. The principal conclusions of Reinleitner et al. [1983] are qualitatively confirmed, except for the interpretation of the particular instabilities involved in the electrostatic

bursts. It is shown that the electron-ion two stream instability dominates except as possibly associated wtih the chorus hooks.

The theory of the instabilities is developed in Section II. A discussion of the predictions and the data, as well as the physical mechanisms, is given in Section III. The results are summarized in Section IV.

II. THEORETICAL MODEL

One example of the electron distribution function seen when chorus and the electrostatic bursts are present is presented in Figure 1. It consists of the following components:

(1) A near Maxwellian central body with a thermal velocity $v_e \sim 5 \times 10^8$ cm/sec. (Note that it does not fit a Lorentzian well—see the difference in the log plots of the distribution in Figure 2.)

(2) Two field aligned beams with beam velocities $v_b \sim \pm 1.6 \times 10^9$ cm/sec.

(3) A non-Maxwellian tail which sets in when $f(v)$ is less than 10^{-4} times its value at the peak, and at a velocity over twice v_b.

Since the non-Maxwellian tail makes only a minor contribution to the distribution function, it should be quite reasonable to neglect it. Thus, we may take the reduced distribution function of the background electrons to be

$$f_e(v) = (1/\sqrt{\pi}v_e)e^{-v^2/v_e^2} \tag{1}$$

where v is the velocity along the field. The ions will also be taken to be Maxwellian. The beam electrons will be taken to be a square distribution:

$$f_b(v) = \begin{cases} A & \sqrt{v_b^2 - 2e\phi/m_e} < v < \sqrt{v_b^2 + 2e\phi/m_e} \\ 0 & \text{otherwise} \end{cases} \tag{2}$$

where v_b is equal to the phase velocity of the chorus wave ω/k, and ϕ is the wave potential. If we take the width of the beam in velocity space to be $2\Delta v$, where Δv is the beam thermal velocity, then $A = 1/2\Delta v$.

The electrostatic beam modes that can be present are primarily magnetic field aligned, hence they will be taken to satisfy the one-dimensional magnetic-field-free electrostatic dispersion relation:

$$1 = \frac{\omega_{pi}^2}{k^2 v_i^2} Z'\left(\frac{\omega}{kv_i}\right) + \frac{\omega_{pe}^2}{k^2 v_e^2} Z'\left(\frac{\omega}{kv_e}\right) + \frac{\omega_{be}^2}{k^2 \Delta v^2} \int \frac{\partial f_b/\partial v}{v - \omega/k} \, dv \tag{3}$$

where $\omega_{p\alpha}^2 = n_\alpha e^2/m_\alpha \varepsilon$, $\omega_{be}^2 = n_b e^2/m_e \varepsilon_0$ and n_i, n_e and n_b denote the background ion and electron and electron beam densities, respectively. Here $Z(\zeta)$ is the familiar plasma dispersion function. The last integral is straightforward to evaluate from Equation 2. The beam modes in Equation 3 satisfy $\omega_r/k \sim v_b$ (where $\omega = \omega_r + i\gamma$), and for the chorus trapped electron beams $v_b^2 \gg v_i^2$, so that we may use the large argument expansion of the plasma dispersion function for the ions [Fried and Conte, 1964]:

$$Z'(\zeta) \overset{\zeta \gg 1}{\sim} -2i\sqrt{\pi}\zeta e^{-\zeta^2} + \frac{1}{\zeta^2}\left(1 + \frac{3}{2\zeta^2} + \ldots\right) \tag{4}$$

Thus, the dispersion relation becomes

$$1 \simeq \frac{\omega_{pe}^2}{k^2 v_e^2} Z'\left(\frac{\omega}{kv_e}\right) + \frac{\omega_{pi}^2}{\omega^2} - 2i\left(\frac{\omega\omega_{pi}^2}{k^3 v_i^3}\right)\sqrt{\pi}\, e^{-\omega^2/k^2 v_i^2} + \frac{\omega_{be}^2}{(\omega - kv_b)^2 - k^2\Delta v^2} \; . \tag{5}$$

We will consider the solution in two particular cases [Briggs, 1964].

(1) Resistive medium instability ($v_e > v_b > \sqrt{m_e/m_i}\, v_e$)

Assume $v_e^2 \gg v_b^2$ (i.e., $v_e \gtrsim 3 v_b$) to simplify the problem. Then the small argument expansion of the plasma dispersion function may be used

$$Z'(\zeta) \overset{\zeta \ll 1}{\sim} -2\sqrt{\pi}\, i\zeta e^{-\zeta^2} -2(1 - 2\zeta^2 + \ldots) \qquad . \tag{6}$$

Then Equation 5 becomes

$$1 + \frac{2\omega_{pe}^2}{k^2 v_e^2} - \frac{\omega_{pi}^2}{\omega^2} + 2\sqrt{\pi} i \left[\left(\frac{\omega\omega_{pe}^2}{k^3 v_e^3}\right)e^{-\omega^2/k^2 v_e^2} + \right. \tag{7}$$

$$\left.\left(\frac{\omega\omega_{pi}^2}{k^3 v_i^3}\right) e^{-\omega^2/k^2 v_i^2}\right] \simeq \frac{\omega_{be}^2}{(\omega - kv_b)^2 - k^2\Delta v^2} \qquad . $$

This can be solved in a straightforward manner to give

$$\omega = kv_b \pm \left(k^2 \Delta v^2 + \frac{\omega_{be}^2}{g + iD}\right)^{1/2} \tag{8}$$

where

$$g = 1 + \frac{2\omega_{pe}^2}{k^2 v_e^2} - \frac{\omega_{pi}^2}{k^2 v_b^2} \tag{9}$$

and

$$D = 2\sqrt{\pi}\left[\left(\frac{\omega_{pe}^2}{\omega^2}\right)\left(\frac{v_b^3}{v_e^3}\right) e^{-v_b^2/v_e^2} + \left(\frac{\omega_{pi}^2}{\omega^2}\right)\left(\frac{v_b^3}{v_i^3}\right) e^{-v_b^2/v_i^2}\right] \tag{10}$$

$$\simeq 2\sqrt{\pi}\left(\frac{\omega_{pe}^2}{\omega^3}\right)\left(\frac{v_b^3}{v_e^3}\right) e^{-v_b^2/v_e^2} \quad .$$

The neglect of the ion contribution to D is justified since $v_b^2 \gg v_i^2$. Now Equation 8 can be further simplified since $D^2 \ll g^2$, allowing a separation of the real and imaginary parts:

$$\omega_r \simeq k v_b \mp \left[k^2 \Delta v^2 + \frac{\omega_{be}^2}{(1 + 2\omega_{pe}^2/k^2 v_e^2 - \omega_{pi}^2/k^2 v_b^2)}\right] \qquad (11)$$

$$\gamma \simeq \frac{\pm \sqrt{\pi}\, \omega_{be}^2 (v_b^3/v_e^3)(\omega_{pe}^2/\omega_r^2) e^{-v_b^2/v_e^2}}{\left[1 + 2(\frac{\omega_{pe}^2}{\omega_r^2})(\frac{v_b^2}{v_e^2}) - (\frac{\omega_{pi}^2}{\omega_r^2})\right]^{3/2} \left[\omega_{be}^2 + \omega_r^2(\frac{\Delta v^2}{v_b^2})(1 + 2\frac{\omega_{pe}^2 v_b^2}{\omega_r^2 v_r^2} - \frac{\omega_{pi}^2}{\omega_r^2})\right]^{1/2}}$$

$$(12)$$

The top signs represent the unstable mode of interest. Growth rate $\gamma(\omega_r)$ is plotted for various ratios v_b/v_e and a couple of different ratios $\eta \equiv \omega_{be}^2/\omega_{pe}^2 = n_b/n_e$ in Figures 3 and 4.

It is clear from the plots that the frequency at which the growth rate is maximum increases with increasing v_b/v_e and η. This relationship can be made explicit by setting $\partial\gamma/\partial\omega_r = 0$ and solving for ω_r. If we denote the resulting ω_r by ω_{max} (i.e., the frequency which maximizes γ), the result is

$$\frac{\omega_{max}^2}{\omega_{pe}^2} = \frac{-(\eta + 3\frac{\Delta v^2}{v_e^2}) + \left[(\eta + 3\frac{\Delta v^2}{v_e^2})^2 + 8(\frac{\Delta v^2}{v_e^2})(\eta + 2\frac{\Delta v^2}{v_e^2})\right]^{1/2}}{4(\frac{\Delta v^2}{v_b^2})} \qquad (13)$$

Thus ω_{max} is a function of three ratios: $(\Delta v/v_b)$, (v_b/v_e) and η.

In the case that is being considered here, $v_t/v_e < 1$, the beams are very difficult to separate from the bulk of the distribution function since they occur close to the center of the distribution function. In addition, these electron beams are expected to be highly variable in time so that they will often not be sampled by the LEPEDEA plasma instrument. However, Equation 13 combined with other indirect data may be adequate to determine the properties of such electron beams in the resistive medium case. v_e can be estimated from the LEPEDEA data. Δv can be estimated from the amplitude of the potential or electric field of the chorus [see Equation 2]. ω_{pe} can be estimated from the continuum radiation cutoff (which is just another measurement of the electron density), and ω_{max} is determined by the maximum in the spectrum of the electrostatic bursts. Since Equation 13 is not very sensitive to η it can be used to predict the beam velocity v_b. If, on the other hand, we estimate v_b from the chorus phase velocity, which is determined from the whistler dispersion relation and the local electron plasma density and magnetic field, the spectral maximum may provide an estimate of η and hence the beam density n_b. Thus, the electrostatic spectrum may provide a diagnostic for one of the beam properties in those cases for which the beam is obscured by being too close to the center in the LEPEDEA data.

In Figure 5 we have plotted ω_{max}/ω_{pe} as a function of v_b/v_e for $v_b/v_e < 0.5$ and different values of η. The plot exhibits the monotone increase of ω_{max} with v_b/v_e, as well as with η, although the latter is minor when v_b/v_e is small. The plot is also very suggestive that ω_{max} approaches ω_{pe} as v_b/v_e approaches 1.

2. Electron-ion two stream instability ($v_e < v_b$)

This is the case exhibited in Figure 1, and is just the well-known beam plasma instability. The case will be treated here as a review for those who may be unfamiliar with this beam instability. We will assume $v_b^2 \gg v_e^2$ to simplify the analysis. Then we may use the small argument approximation, Equation 4, to the plasma dispersion function in Equation 5 to obtain the dispersion relation:

$$
1 \simeq \frac{\omega_{pe}^2}{\omega^2}\left(1 + \frac{3}{2}\frac{k^2 v_e^2}{\omega^2}\right) + \frac{\omega_{pi}^2}{\omega^2} + \frac{\omega_{be}^2}{(\omega - kv_b)^2 - k^2\Delta v^2}
$$

$$
- 2\sqrt{\pi}i\left[\left(\frac{\omega\omega_{pe}^2}{k^3 v_e^3}\right)e^{-\omega^2/k^2 v_e^2} + \left(\frac{\omega\omega_{pi}^2}{k^3 v_i^3}\right)e^{-\omega^2/k^2 v_i^2}\right] \tag{14}
$$

This can be rewritten in the form

$$
(\omega - kv_b)^2 = k^2\Delta v^2 + \frac{\omega_{be}^2}{h(\omega) + i\mathcal{D}} \tag{15}
$$

where

$$
h(\omega) = 1 - \frac{\omega_{pe}^2}{\omega^2}\left(1 + \frac{3}{2}\frac{k^2 v_e^2}{\omega^2}\right) - \frac{\omega_{pi}^2}{\omega^2} \tag{16}
$$

and $\mathcal{D}$ is given by Equation 10.

A close inspection of Equation 15 shows that for $\Delta v^2/v_b^2 \ll 1$ and $\eta = n_b/n_e \ll 1$ there is only a solution if $\omega \simeq kv_b$. This allows one to expand $h(\omega)$:

$$h(\omega) \simeq h(kv_b) + (\omega - kv_b)h'(kv_b) \tag{17}$$

Now for $k^2v_b^2 \ll \omega_{pe}^2$ we have

$$\frac{|h(kv_b)|}{|h'(kv_b)|} \simeq 2\omega \gg |\omega - kv_b| \tag{18}$$

Thus, in that case the second term of Equation 17 is totally negligible. However, for $kv_b \sim \omega_{pe}$, $h(kv_b) \ll 1$ and the second term of Equation 17 is not negligible. In both cases $h(\omega) < 0$ and the right-hand side of Equation 15 is negative for $\Delta v^2/v_b^2 < \eta$, so that an instability exists for all ω to ω_{pe} provided that criterion is satisfied. For $kv_b > \omega_{pe}$, the right-hand side is positive, so only a stable propagating mode with normal Landau damping occurs.

For $k^2v_b^2 \ll \omega_{pe}^2$ we have $h(\omega) \simeq h(kv_b)$ and $|h(kv_b)| \gg D$, so that

$$\omega_r \simeq kv_b + O(\eta D/h^2) \tag{19}$$

$$\gamma \simeq k\{\eta v_b^2/[1 + \frac{3}{2}(\frac{v_e^2}{v_b^2})] - \Delta v^2\}^{1/2} \tag{20}$$

For $kv_b \sim \omega_{pe}$,

$$h(\omega) \simeq h(\omega_{pe}) + (\omega - \omega_{pe})h'(\omega_{pe})$$

(21)

$$\simeq [- \frac{3}{2}(\frac{v_e^2}{v_b^2}) + \frac{(\omega - \omega_{pe})}{\omega_{pe}}] \quad .$$

If we substitute this back into Equation 15 and set $\delta = \omega - \omega_{pe}$, we obtain the cubic equation:

$$2\delta^3 - (\frac{3v_e^2}{2v_b^2} - iD) \omega_{pe}\delta^2 - 2k^2\Delta v^2\delta - \omega_{pe}(\eta \omega_{pe}^2 + iD k^2\Delta v^2) = 0 \quad (22)$$

Equation 22 can be solved by perturbation methods to give

$$\omega_r \simeq \omega_{pe}[1 + \frac{v_e^2}{2v_b^2} - (\frac{2}{\eta})^{1/3} \frac{\Delta v^2}{3v_b^2} - \frac{1}{2}(\frac{\eta}{2})^{1/3}] \quad (23)$$

$$\gamma \simeq \omega_{pe}[\frac{\sqrt{3}}{2}(\frac{\eta}{2})^{1/3} - \frac{D}{3} - \sqrt{3}(\frac{2}{\eta})^{1/3} \frac{\Delta v^3}{3v_b^2}] \quad (24)$$

D is just the normal (electron Landau damping, given by Equation 10.

Equation 23 gives the frequency at which the growth rate is a maximum, so that it is analogous to Equation 13. This is plotted as a

function of v_b/v_e for various η in Figure 6. In principal, one might

use the theoretical prediction to try to extract information on the

beam from the spectrum. But in this case, the beam characteristics

show up quite clearly in the particle data, as in Figure 1. Comparison

of Figure 6 with Figure 5 shows that ω_{max} switches from an increasing

function of v_b/v_e to a decreasing function near $v_b/v_e \sim 1$.

III. DISCUSSION

The electron distribution function shown in Figure 1 has $v_b/v_e \sim$
3. The wave spectrum during the same interval is shown in Figure 8.
The peak in the intensity occurs near $f \simeq 6$ Hz, or $f/f_{pe} = \omega/\omega_{pe} \simeq$
1.0. This spectrum runs from about 0.9 f_{pe} up to 1.1 f_{pe}. This is to
be compared with the frequency of the growth rate maximum of $\omega_r \sim 0.97$
ω_{pe} predicted by Equation 23 for the beam plasma instability if we
estimate $\eta \sim 10^{-3}$ from Figure 1. Thus, this case is in good agreement
with predictions of the beam-plasma or electron-ion two-stream insta-
bility. The spectrum of electrostatic noise is seen to be associated
primarily with an intensification of the chorus waves and not with the
chorus hooks. Another example of this case of bursts associated with
chorus band intensification was shown in Figure 2 of Reinleitner et al.
[1983]. The spectrum runs up to f_{pe} with a peak near 0.8 f_{pe}, consis-
tent with the beam plasma instability.

Several examples of electrostatic bursts associated with chorus
hooks were given in Reinleitner et al. [1983]. The spectrum in this
case is different than for the chorus intensification associated
bursts. The spectrum does not usually extend up to the plasma fre-
quency, and often peaks near 0.5 f_{pe} or less. Furthermore, the bursts
tend to be short-lived, normally having a lifetime of a second or less.
The spectrum is consistent with a resistive medium instability or an

instability on the transition between resistive medium and beam-plasma
(see Figures 3, 4, and 5).

The reasons for the two different types of bursts, apparently
associated with two distinct characteristic chorus waves, can be
explained as follows. When the chorus hooks are present, the spectrum
is spreading rapidly to higher frequencies. As this happens, $\omega/k \sim \sqrt{\omega}$
also increases rapidly, trapping and accelerating particles in the
right velocity range. In this case, the frequency at the beginning of
the hook may be sufficiently low that ω/k lies more on the main part of
the distribution function than the tail. Since the phase velocity
changes rapidly the wave quickly traps and accelerates enough particles
to create a significant bump in velocity space before moving very far
in velocity space. Thus, $v_b \lesssim v_e$ when the instability develops. After
ω ceases to rise, the trapping rate drops drastically, the particle
"bump" quickly becomes detrapped, and the instability ceases.

In the case of the electrostatic noise associated with intensifi-
cations of the chorus, the frequency of the chorus is normally 2 or 3
times that at the beginning of the chorus hooks. Thus, the wave phase
velocities may lie more on the tail of the distribution function at the
outset, and get accelerated more slowly by gradients in the Earth's
magnetic field. The number of trapped particles may be smaller than
that of the case of the chorus hooks. When the chorus intensifies, it
can pass the threshold (growth exceeds damping) of the beam plasma
instability. While the trapped beam particles become untrapped and
relax to lower energies due to quasilinear effects, the chorus wave is

continually trapping and accelerating particles to regenerate the beam. Thus, the instability persists as long as the chorus does.

The results of this paper can be compared to those of Reinleitner et al. [1983] in which a model of a Lorentzian electron distribution and a cold beam were assumed. First of all, the use of a Lorentzian electron distribution causes an overestimation of the growth rate for the resistive medium instability. Secondly, the neglect of beam thermal effects overestimates the beam plasma instability growth rate, although the error is rather small near the peak growth rate. Thirdly, the position of the peaks compares favorably with that of the present model for the resistive medium case, but not as well for the beam-plasma case. The reason for the latter discrepancy is that a Lorentzian distribution does not properly treat the thermal effects for frequencies near the plasma frequency. Equation 14 should be the more accurate expression of the peaks for the resistive medium case and Equation 23 a useful expression for the peaks of the beam plasma case. Overall, however, the Reinleitner et al. model gives a good qualitative estimate of the principal features of the instability.

IV. SUMMARY AND CONCLUSIONS

The growth rates for a finite temperature beam of chorus trapped electrons in a Maxwellian plasma were determined for both the resistive medium ($v_b < v_e$) and beam plasma ($v_b > v_e$) instability cases. These results are qualitatively in good agreement with those of Reinleitner et al. [1983], except in the conclusion as to the relative importance of the two mechanisms. The beam plasma (electron-ion two stream) instability was found to be associated with the long time electrostatic bursts generated during the gradual intensifications of the chorus. A border-line resistive medium or a transitional resistive-medium beam-plasma instability is associated with the chorus hooks. The physical reason for the apparently different mechanisms in the two cases was explained in terms of the initial phase velocity of the wave and the acceleration mechanisms in each case.

For the case of the chorus hooks, beams are normally not detectable in the particle data. The maximum growth rate was determined as a function of the ratios of beam and electron thermal velocity to beam velocity and beam density to plasma density for the case of a resistive insta-bility. This may allow the observed peak in the electrostatic noise spectrum to be used as a diagnostic for beam properties in this case. In particular, everything in the expression for the maximum growth rate is capable of being estimated except possibly the beam velocity or the beam density. Thus, the spectrum may be used as a diagnostic for beam velo-city or density in such cases.

ACKNOWLEDGEMENTS

REFERENCES

Briggs, R. J., Electron-Stream Interactions With Plasmas, MIT Press, Cambridge, Mass., 1964.

Fried, B., and S. Conte, The Plasma Dispersion Function, Academic Press, New York, New York, 1961.

Gurnett, D., and L. Reinleitner, Electron acceleration by Landau resonance with whistler mode wave packets, Geophys. Res. Lett., in press, 1983.

Reinleitner, L., D. Gurnett, and T. Eastman, Electrostatic bursts generated by electrons in Landau resonance with whistler mode chorus, J. Geophys. Res., 88, 3079, 1983.

Reinleitner, L., D. Gurnett, and D. Gallagher, Chorus-related electrostatic bursts in the earth's outer magnetosphere, Nature, 295, 46, 1982.

FIGURE CAPTIONS

Figure 1   Perspective plot of the electron distribution in velocity

space on August 10, 1979, from 1353-1355 UT, determined

by ISEE-1 LEPEDEA data.

Figure 2   Log plots of the Lorentzian and Maxwellian distribution

functions. The Maxwellian curves in while the Lorentzian

curves out.

Figure 3   Plot of the growth rate γ as a function of v_b/v_e for the

negative energy or resistive medium beam instability, for

$\eta = 10^{-3}$.

Figure 4   Plot of the growth rate γ as a function of v_b/v_e for the

negative energy or resistive medium beam instability, for

$\eta = 2 \times 10^{-2}$.

Figure 5   Plot of the frequency of maximum growth rate ω_{max} as a

function of v_b/v_e for the resistive medium instability.

Figure 6   Plot of the frequency of maximum growth rate ω_{max} as a

function of v_b/v_e for beam-plasma instability.

Figure 7   Wave spectrum from the SFR instrument during the time

period of Figure 1.

C-G82-606

ISEE -1
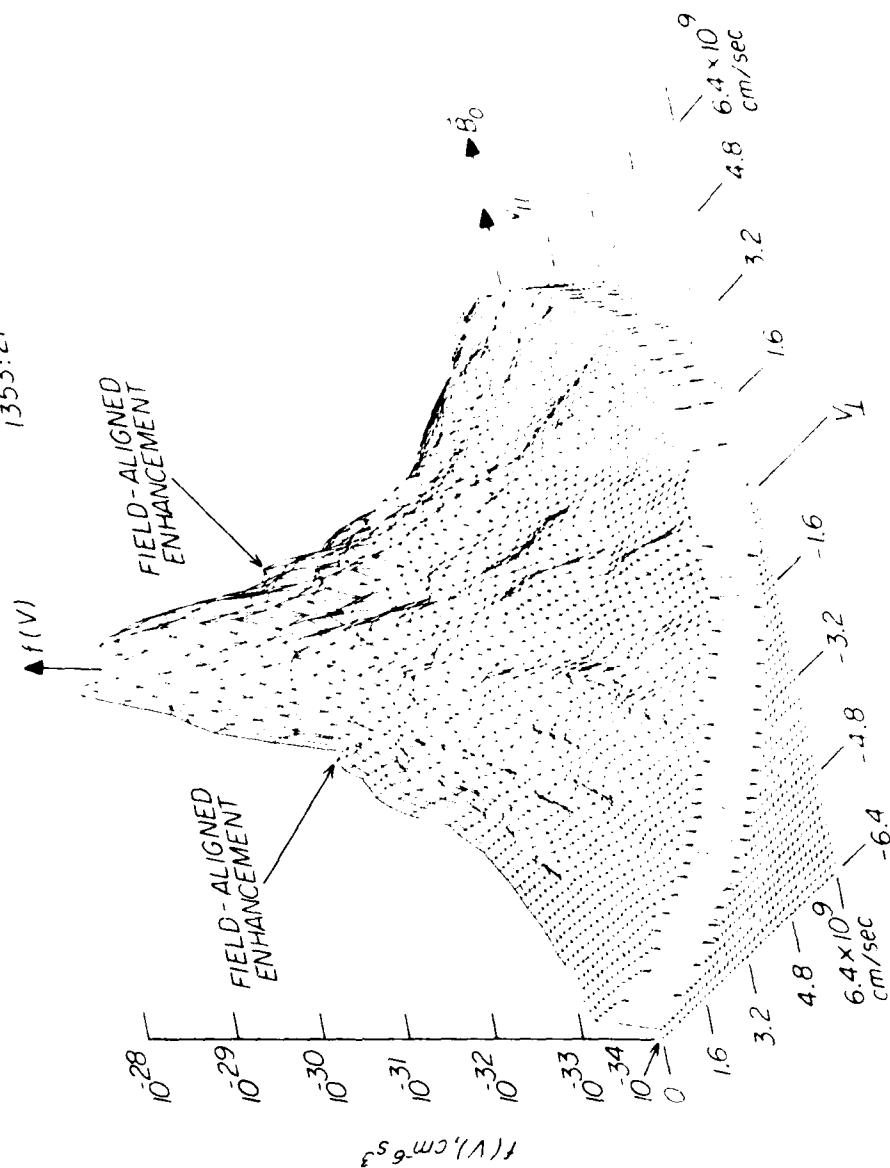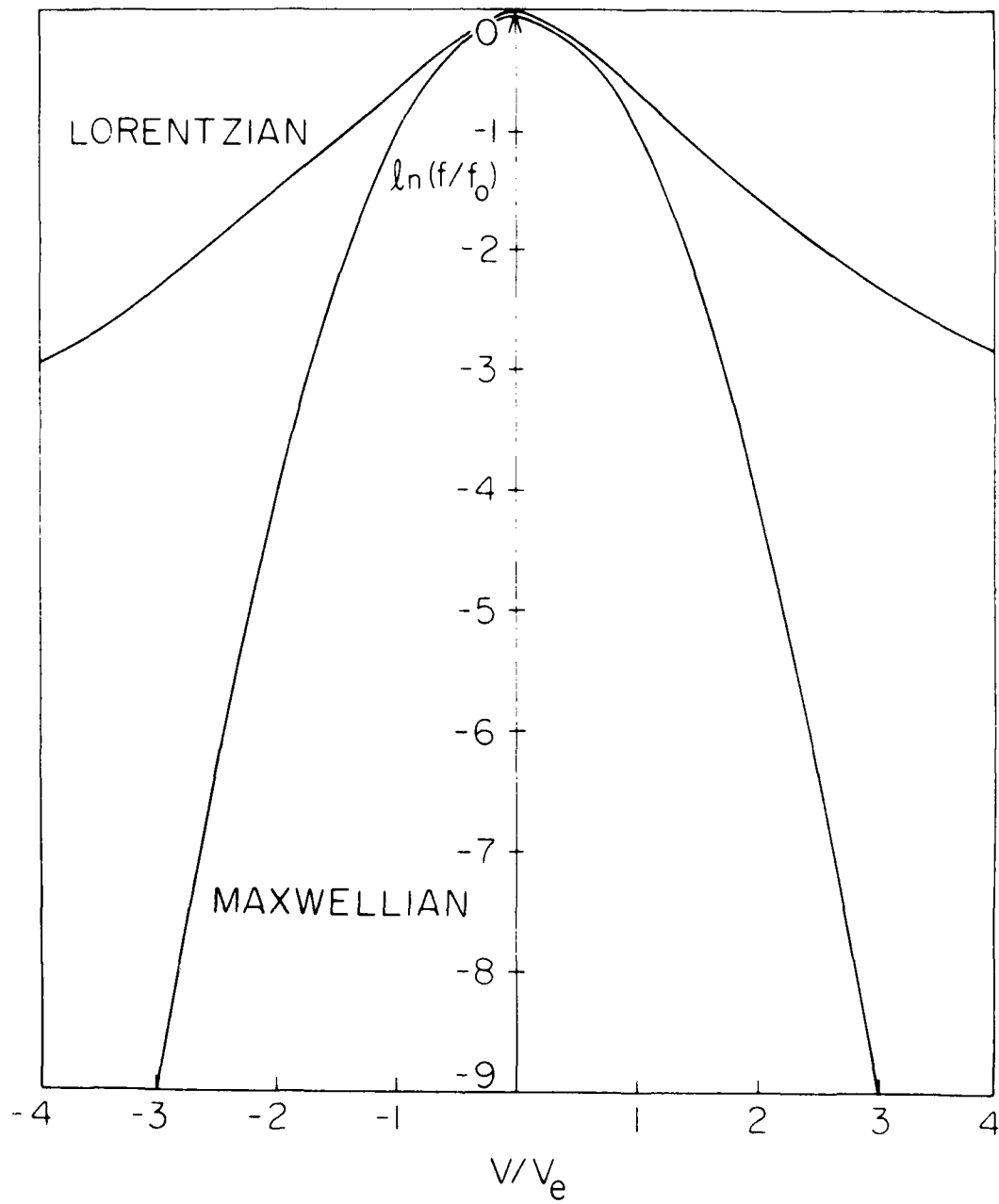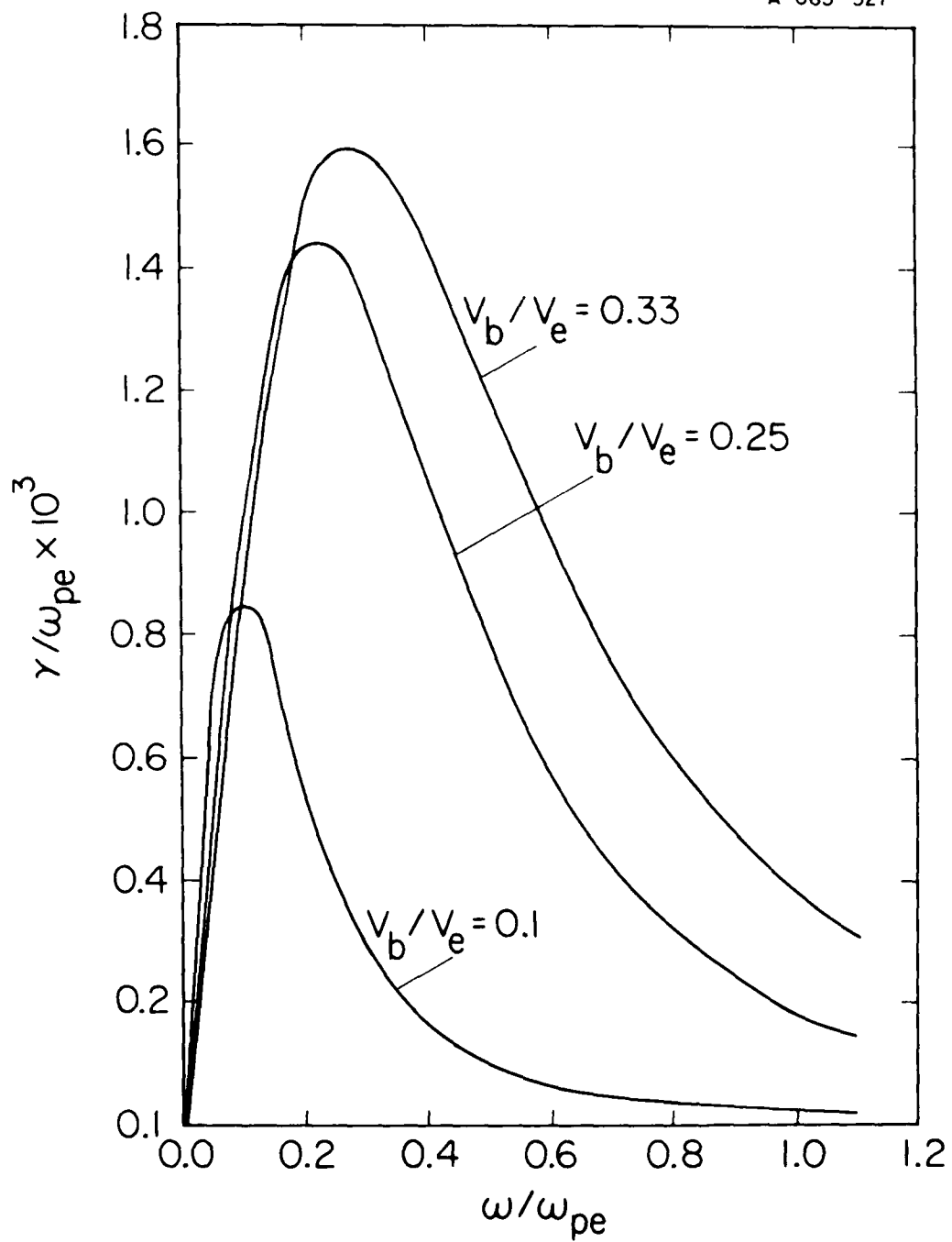IO AUGUST 1979
1353:21 - 1355:29 UT

FIELD - ALIGNED
ENHANCEMENT

FIELD - ALIGNED
ENHANCEMENT

Figure 1

Figure 2

A-G83-527

Figure 3

Figure 4

A-G83-526

$\eta = 10^{-1}$
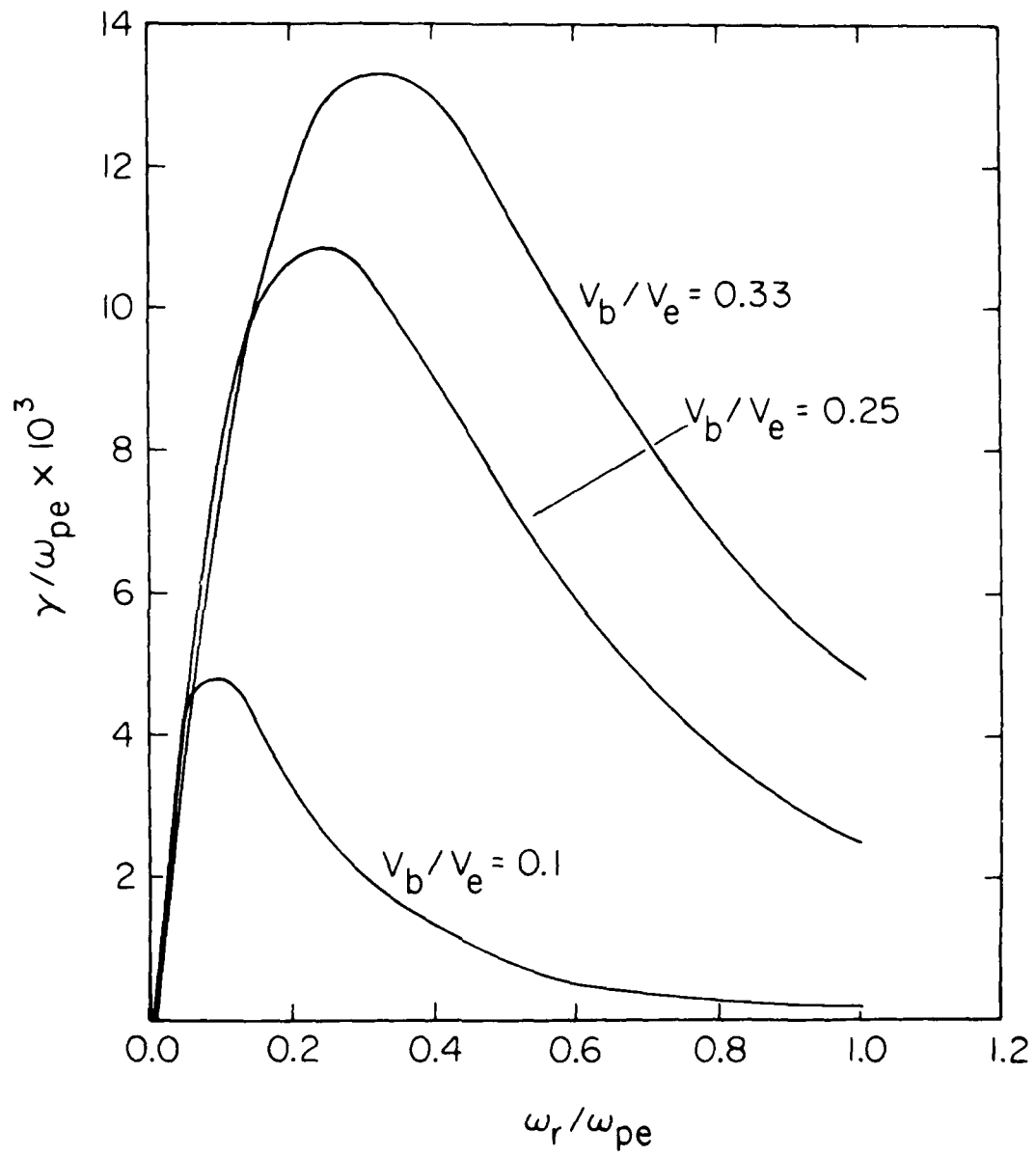
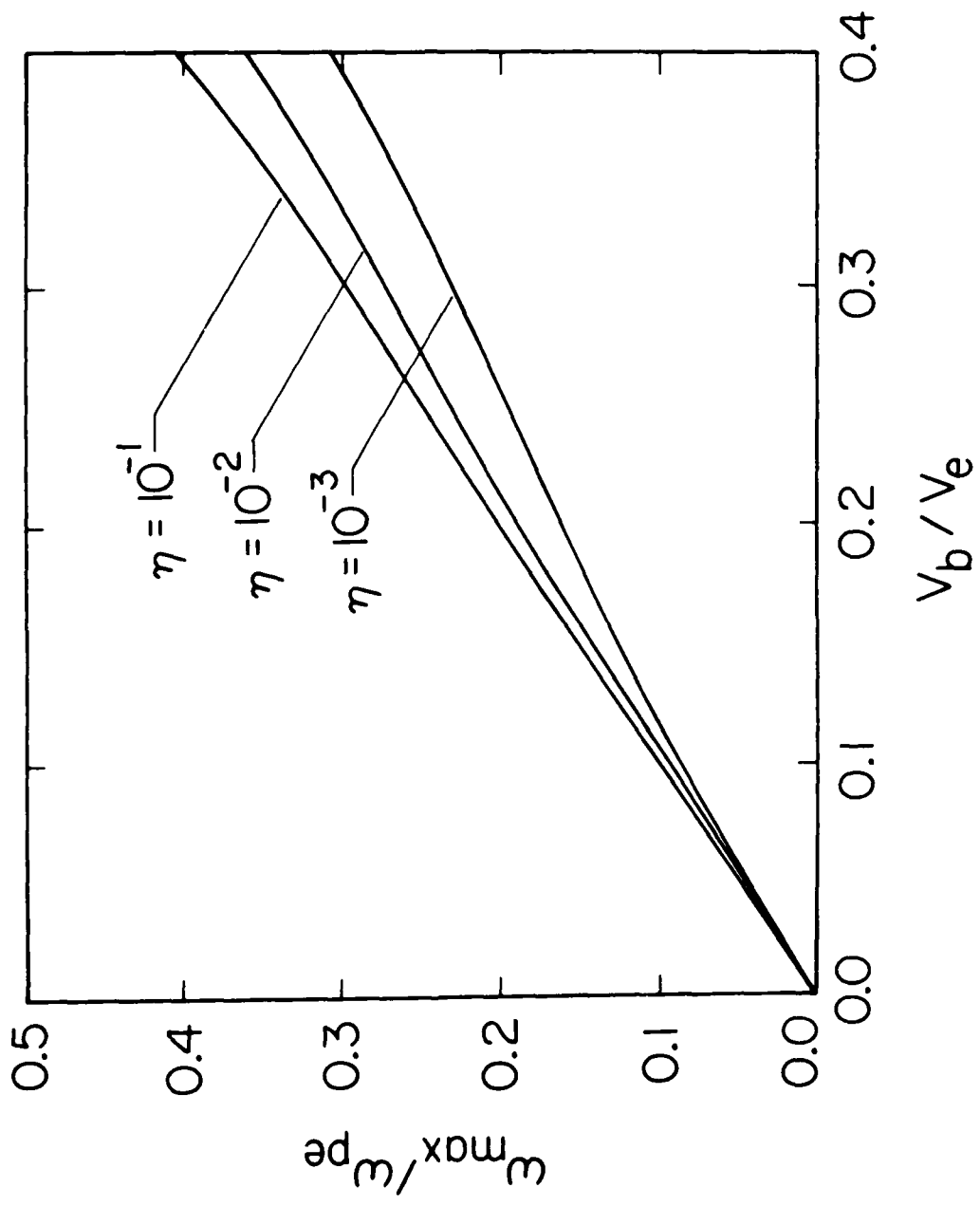$\eta = 10^{-2}$

$\eta = 10^{-3}$

V_b / V_e

$\omega_{max} / \omega_{pe}$

Figure 5

A-G83-579
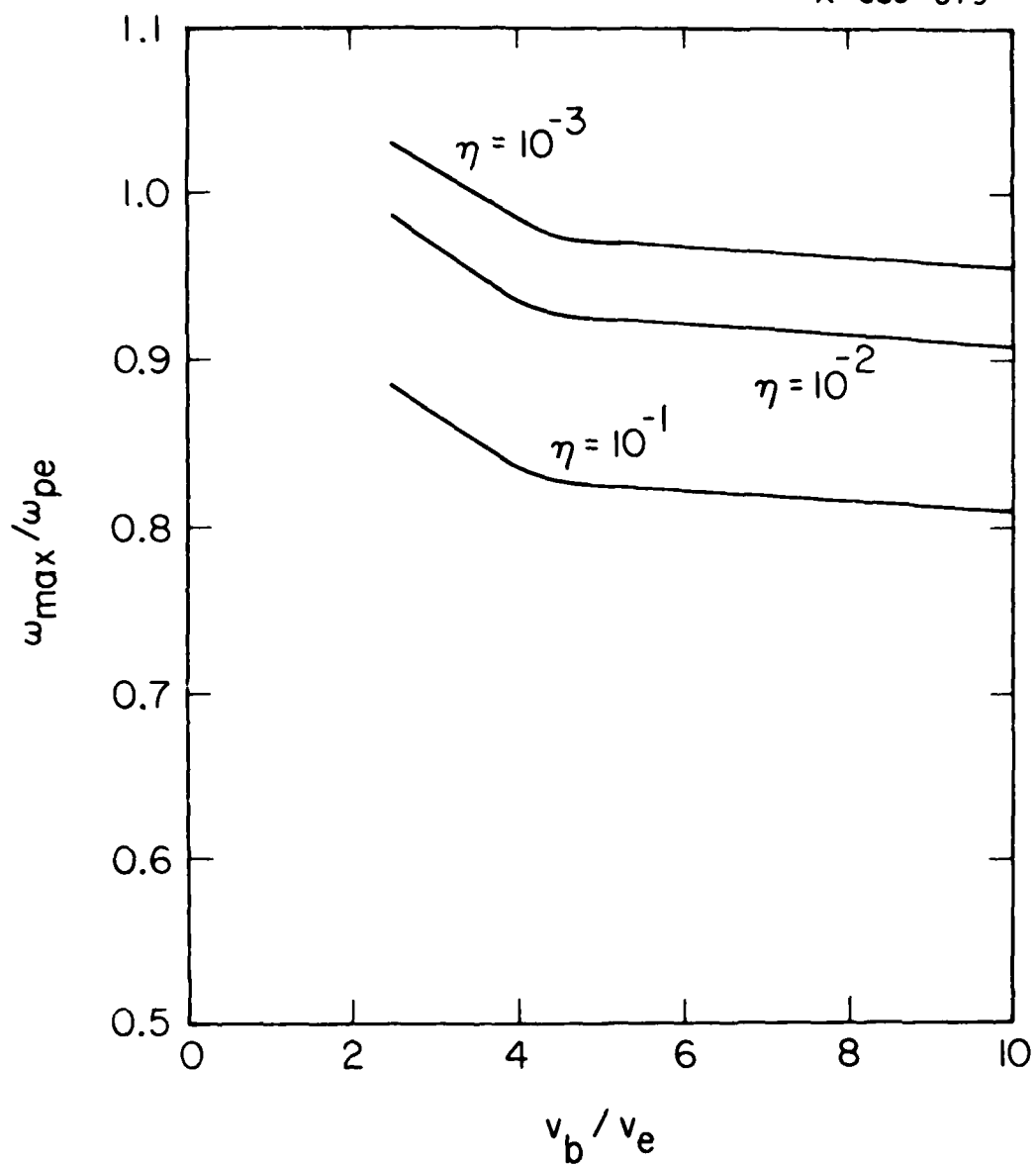
Figure 6

ISEE I AUGUST 10, 1979 DAY 222
R = 12.9 R_E MAG LAT = -21.4° MLT = 16.3 HRS

B-G83-538-I

CHORUS BAND

ELECTROSTATIC BURSTS

FREQUENCY (kHz)

UNIVERSAL TIME

Figure 7